Supporting Information

Functional role of solvent entropy and conformational entropy of metal binding in a dynamically-driven allosteric system

Daiana A. Capdevila[1], Katherine A. Edmonds[1], Gregory C. Campanello[1,2], Hongwei Wu[1], Giovanni Gonzalez-Gutierrez[3] and David P. Giedroc[1,3]*

[1]Department of Chemistry, Indiana University, Bloomington, IN 47405-7102 USA

[2]Present address: Department of Biological Chemistry, University of Michigan Medical Center, Ann Arbor, MI 48109-0600 USA

[3]Department of Molecular and Cellular Biochemistry, Indiana University, Bloomington, IN 47405 USA

This file contains Supporting Table S1-S5, Supporting Figures S1-S13 and Appendix 1-2.

This Supporting Information includes:

Supporting Tables

Table S1. Thermodynamic parameters for Zn binding to CzrAs.

CzrA	Affinities at 25.0 °*C* (x10^{12} M^{-1}) [b]	Zn binding at 25.0 °*C*				
		ΔG_{TOT} (kcal/mol) [b]	ΔH_{TOT} (kcal/mol) [b]	$-T\Delta S_{TOT}$ (kcal/mol) [b]	$-T\Delta S_{CONF}$ (kcal/mol) [c]	$-T\Delta S_{SOLV}$ (kcal/mol)
wild-type[a]	$K_1 = 11 \pm 1$ $K_2 = 1.63 \pm 0.07$	–33.0 ± 0.4	–4.2 ± 0.7	–28.8 ± 0.7	3.0 ± 0.4	–31.7 ± 1.1 [e]
V66A/ L68A[a]	$K_1 = 1.25 \pm 0.07$ $K_2 = 0.23 \pm 0.06$	–32.0 ± 0.2	2.9 ± 0.1	–34.9 ± 0.2	1.3± 0.25	–33.2 ± 0.5 [d]
V66A[a]	$K_1 = 5 \pm 1$ $K_2 = 1.43 \pm 0.08$	–33.9 ± 0.2	0.1 ± 0.1	–34.0 ± 0.1	6.8 ± 0.9	–40.2 ± 0.6 [d]
V66A/ L68V[a]	$K_1 = 5 \pm 1$ $K_2 = 1.0 \pm 0.1$	–33.7 ± 0.2	–2.2 ± 0.2	–31.5 ± 0.1	–1.2 ± 0.1	–27.5 ± 0.6 [d]
L34A	$K_1 = 4 \pm 1$ $K_2 = 1.2 \pm 0.2$	–33.6 ± 0.4	–5.8 ± 0.5	–27.8 ± 0.5	6.1 ± 0.8	–31.7 ± 0.7 [d]
V66L	$K_1 = 4.0 \pm 0.8$ $K_2 = 0.8 \pm 0.1$	–33.4 ± 0.4	–2.4 ± 0.2	–30.9 ± 0.3	N.D.	N.D.

[a]The corrected ITC values were previously reported[1] and the conformational entropy values were recalculated based on recent recalibration of the "entropy meter"[2]. [b] Values NTA-corrected according to eq. (8).[3] [c] Calculated according to eq. (7).[2] [e] Obtained by difference between $-T\Delta S_{TOT}$ and $-T\Delta S_{CONF}$. [d] Calculated from ΔC_p at 25 °*C* according to Table S5 from equation (4). N.D., no data.

Table S2. Surface accessible area[a] and crystallographic solvation entropies for CzrA variants.

CzrAs	PDB ID (State)	ASA non-polar (Å^2) [a]	ASA polar (Å^2) [a]	Zn binding $-T\Delta S_{SOLV}$ (kcal/mol) [b]	Mutation $-T\Delta S_{SOLV}$ (kcal/mol) [c]
wild-type	1r1u (apo)	5140 ± 50	4570 ± 70	-	-
wild-type	1r1v (Zn)	5140 ± 50	4280 ± 90	-0.5 ± 0.5	-
V66A/L68V	4ggg (Zn)	5080 ± 30	4200 ± 50	-1.2 ± 0.6	-0.6 ± 0.2
L34A	6cda (Zn)	5260	4350	0.6 ± 1.2	1.1 ± 0.2
V66L	6cdb (Zn)	5160 ± 40	4490 ± 60	-0.05 ± 0.51	0.5 ± 0.6

Uncertainties were estimated by averaging the differences from protomers A and B from each crystal structure.
[a]Calculated using the web server for quantitative evaluation of protein structure VADAR 1.8 (vadar.wishartlab.com/)[4] [b]Calculated from eq. (S6) using previously reported empirical parameters[2]. The ΔASA were obtained from each Zn crystal structure against *wild-type* apo protein (1r1u). [b]Calculated from eq. (S6) using previously reported empirical parameters[2]. The ΔASA were obtained from each Zn crystal structure against *wild-type* Zn protein (1r1v).

Table S3. Thermodynamic parameters for DNA binding and heterotropic coupling in CzrA variants obtained from fitting to a single-binding site model coupled to a monomer-dimer equilibrium.

CzrA variant	$K_{DNA,\ apo}$ [a] (x10^9 M^{-1})	$K_{DNA,\ Zn}$ [b] (x10^9 M^{-1})	ΔG_c (kcal mol^{-1})
wild-type	3.6 ± 0.9	0.004 ± 0.002	6.7 ± 0.6 [c]
V66A/L68V	22 ± 10	300 ± 100	1.1 ± 0.6 [c]
L34A	0.6 ± 0.2	20 ± 10 0.18 ± 0.07[a]	0.6 ± 0.8 [c]
V66L	5.1 ± 0.9	0.0031 ± 0.002	7.0 ± 1.0

[a] 0.4 M NaCl, 10 mM HEPES, pH 7.0, 2 mM EDTA [b] 0.23 M NaCl, 10 mM HEPES, pH 7.0, 3 μM $ZnCl_2$ [c]Values previously reported[1].

Table S4. Crystallographic structure data collection and refinement statistics.

	Zn_2 L34A CzrA	Zn_2 V66L CzrA	L34A CzrA Zn[a]
Data collection			
Wavelength (Å)	1.00003	1.00000	1.278180
Space group	P41212	P21212	P41212
Cell dimensions			
a, b, c (Å)	31.99 31.99 183.39	54.55 73.36 50.16	31.99 31.99 183.39
α, β, γ (°)	90.00 90.00 90.00	90.00 90.00 90.00	90.00 90.00 90.00
Resolution (Å)	45.81 – 2.00	41.41 – 1.99	45.83 – 2.08
R_{sym}	0.097 (1.069)	0.067 (0.716)	0.102 (0.514)
R_{meas}	0.101 (1.112)	0.073 (0.782)	0.107 (0.568)
R_{pim}	0.028 (0.304)	0.030 (0.313)	0.031 (0.234)
CC1/2	0.999 (0.878)	0.999 (0.806)	0.998 (0.936)
I/σ(I)	17.6 (2.5)	19.3 (2.4)	11.6 (3.5)
Completeness (%)	96.4 (100.0)	96.1 (100.0)	95.5 (99.1)
Multiplicity	12.4 (12.4)	5.9 (6.2)	11.5 (8.6)
Refinement			
Resolution (Å)	45.85 – 2.0 (2.072 – 2.0)[b]	29.61 – 1.99 (2.14 -1.99)[b]	
No. unique reflections	6867	13796	
R_{work}	0.2167	0.1954	
R_{free}	0.2445	0.2275	
R.m.s.d values			
Bond lengths (Å)	0.008	0.007	
Bond angles (°)	0.877	0.822	
No. atoms			
Protein	766	1525	
Ligand/ions	3	20	
B-factors (Å^2)			
Protein/ligand/ions	35.36	38.33	
Ramachandran plot			

Favored (%)	100	98.9
Allowed (%)	0	1.1
MolProbity score	1.32	1.33
Rotamer outliers (%)	0	0.6
PDB code	6cda	6cdb

[a]Data statistics from crystals used to measure the Zn anomalous scattering sample are shown here. [b]Highest resolution shell values are shown in parentheses.

Table S5. Calorimetric and conformational C_p of CzrAs inferred from ITC and methyl S^2_{axis} dependence on temperature, respectively.

			Zn binding	
CzrA	$C_{p,CONF}$ (apo) (cal mol^{-1}.K^{-1}) [a]	$C_{p,CONF}$ (Zn) (cal.mol^{-1}.K^{-1}) [a]	$\Delta C_{p,CONF}$ (Zn) (cal.mol^{-1}.K^{-1})	$\Delta C_{p,TOT}$ (Zn) (cal.mol^{-1}.K^{-1}) [b]
wild-type	221 $\pm$ 40	248 $\pm$ 40	27 $\pm$ 80	-348 $\pm$ 7
L34A	234 $\pm$ 40	231 $\pm$ 40	3 $\pm$ 80	-375 $\pm$ 9
V66A/L68A	N.D.	N.D.	N.D.	-392 $\pm$ 7
V66A/L68V	N.D.	N.D.	N.D.	-325 $\pm$ 8
V66A	N.D.	N.D.	N.D.	-475 $\pm$ 8

[a]Values were obtained using the methyl S^2_{axis} as a dynamical proxy for protein conformational entropy, eq. 7[2]. [b] Values obtained from $\Delta H_{ITC,1}$ *and* $\Delta H_{ITC,2}$ from fit to a sequential two-site binding model included in the data analysis software provided by MicroCal to the ITC measurements as a function of temperature (see Fig. 5 and Fig. S12).

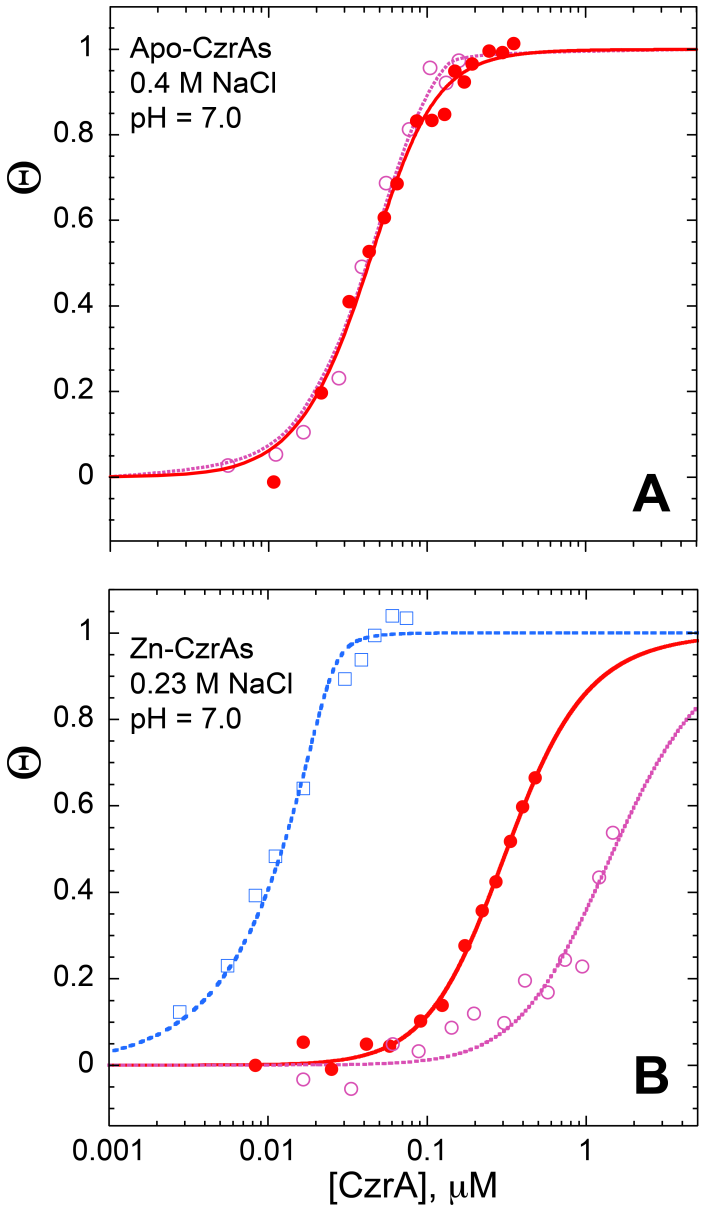

Figure S1. Representative normalized CzrO binding curves for apo (A) and Zn(II) saturated (B) wild-type (red), V66A/L68V (blue) and V66L (violet) CzrAs. The continuous line through each data set represents a nonlinear least square fit to a dissociable dimer model (K_{dim} (Zn-CzrA) = 4.5 x 10^{-5} M^{-1}; K_{dim} (apo-CzrA) = 1.7 x 10^{-5} M^{-1})[5]. Parameters are presented in Table S3. Data for wild-type and V66A/L68V CzrAs are presented for reference and were previously reported[1,6].

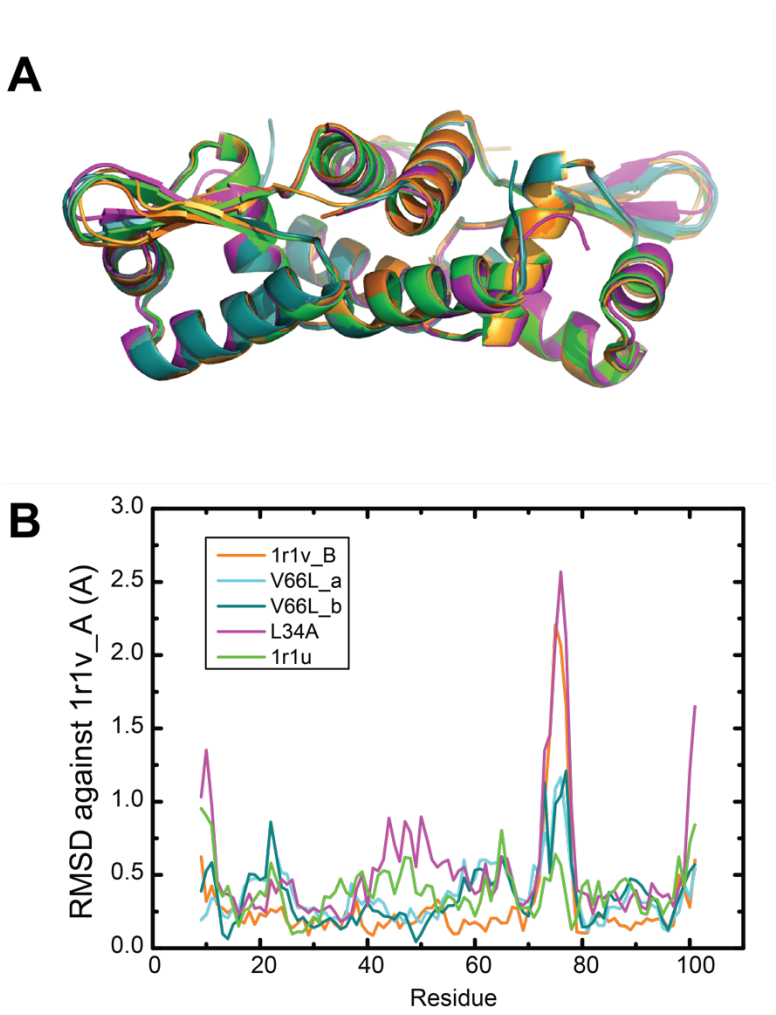

Figure S2. Comparison of crystallographic structures of CzrA variants. (A**)** Superposition of ribbon representation of wild-type Zn-bound CzrA (1r1v, *orange*, chain A) and apo-CzrA (1r1u, chain A&B, *green*), Zn-bound L34A CzrA (6cda, *magenta*) and Zn-bound V66L CzrA (6cdb, *dark green*). See Table S4 for structure statistics for the L34A and V66L CzrAs. **(**B**)** Backbone RMSD (Cα atoms) per residue calculated with VMD.

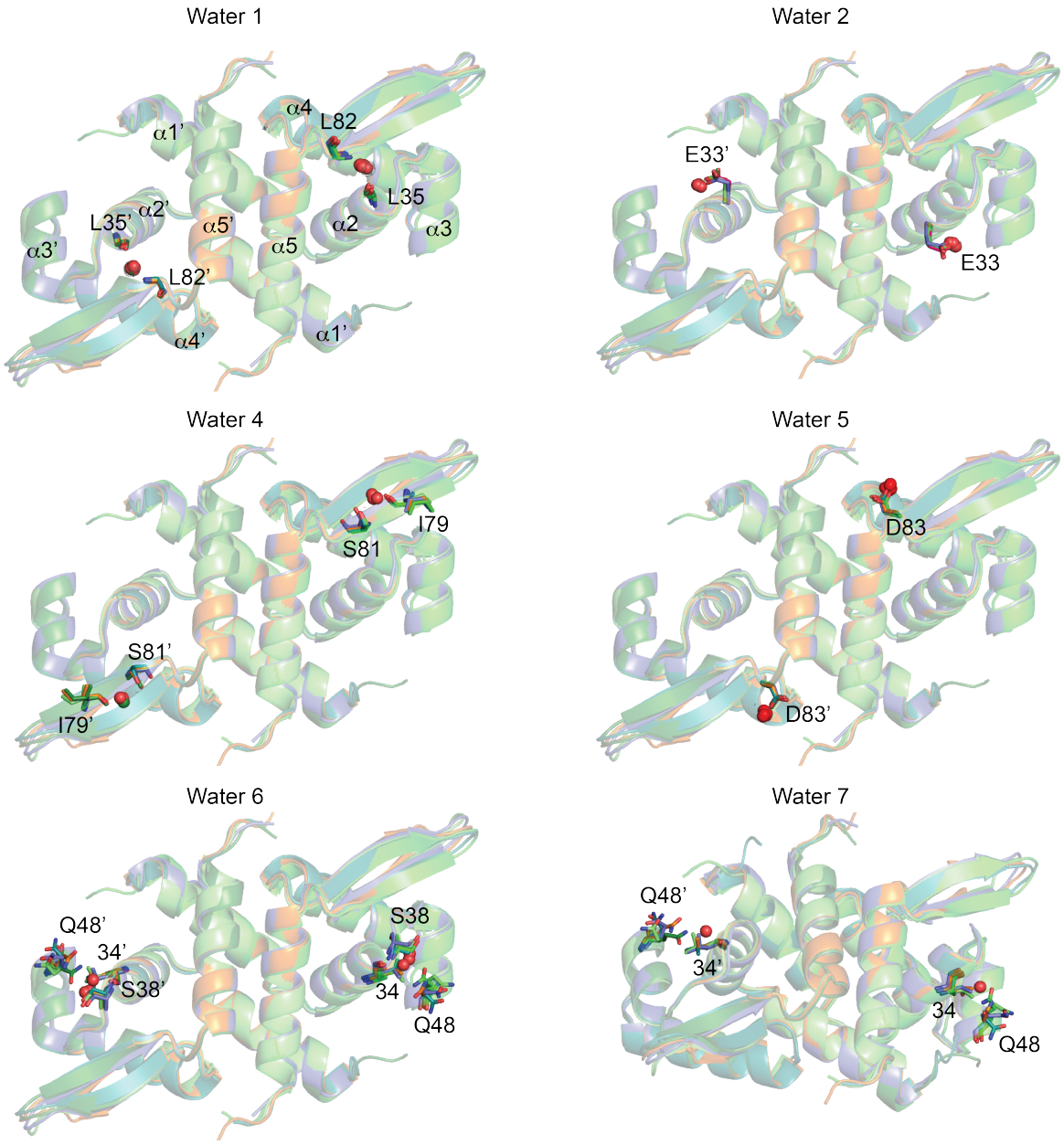

Figure S3. Crystallographic water molecules in CzrAs. These six water molecules were observed with high occupancy in all five crystallographic structures of CzrA in the apo- and Zn states (see Table S2), with the exception of Water 5, which is *not* present in the single apo-CzrA structure (wild-type, pdb code, 1r1u), but is present in all Zn-bound CzrA structures.

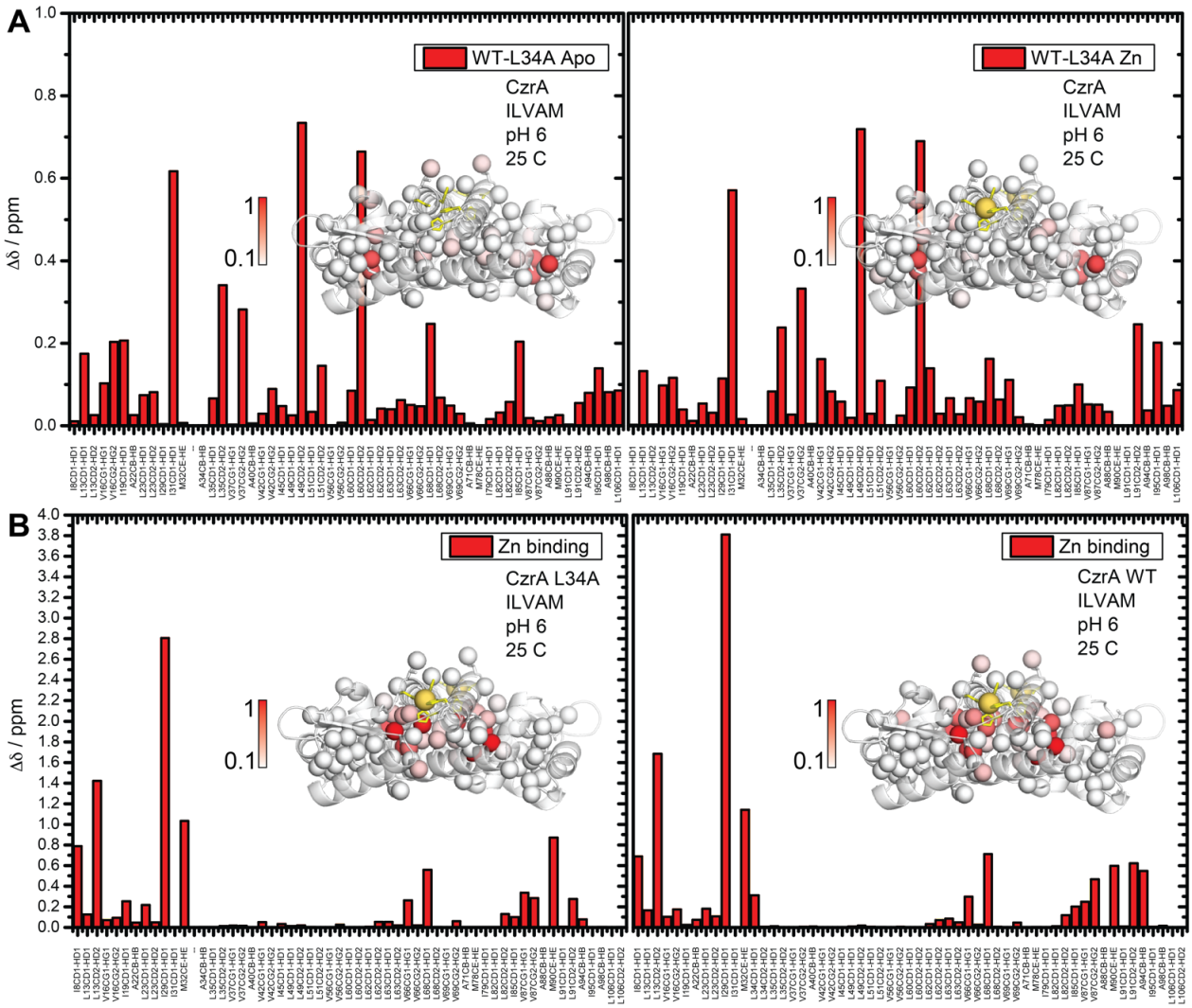

Figure S4. Chemical shift perturbation (csp) maps of wild-type (WT) and L34A CzrAs obtained from assigned spectra in Fig. S5. The ^{13}C-methyl side-chain chemical shift perturbation maps plots that (A) compare apo- (*left*) and Zn-states (*right*) of L34A with wild-type CzrA; and (B) impact of Zn binding on L34A (*left*) and wild-type (*right*) CzrAs. *Insets*, the corresponding csp are painted onto the wild-type CzrA homodimer structure in each panel (PDB ID code 1r1v) with metal-binding residues shown in light yellow.

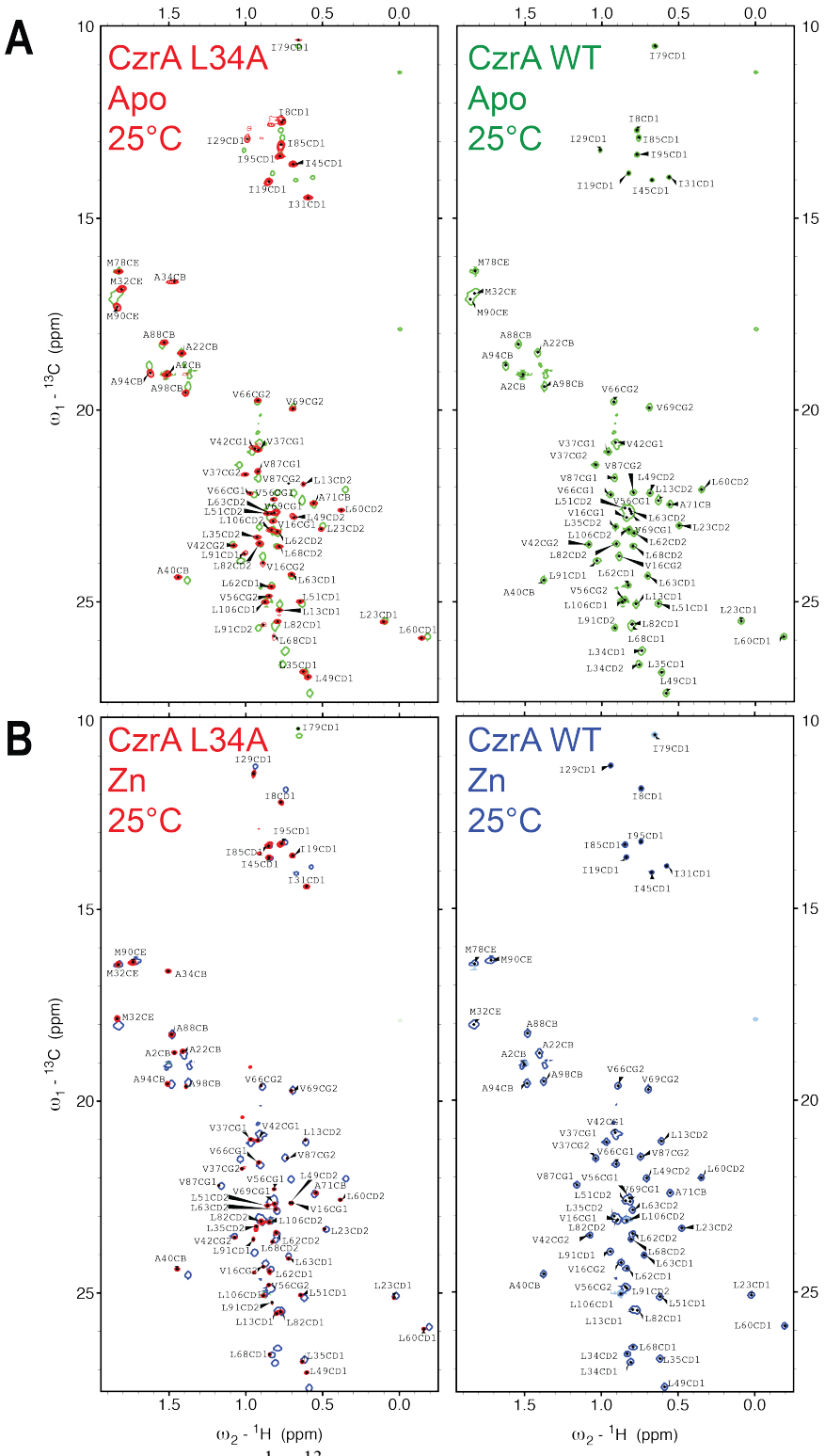

Figure S5. Assigned ^{1}H,^{13}C HSQC spectra of wild-type ILVAM-labeled L34A (left) and wild-type CzrAs (right) in different allosteric states, apo (A), and Zn-bound (B). In the left panels, the spectra of L34A are shown in red contours overlaid on the corresponding WT spectrum shown in green (apo) or blue (Zn-bound).

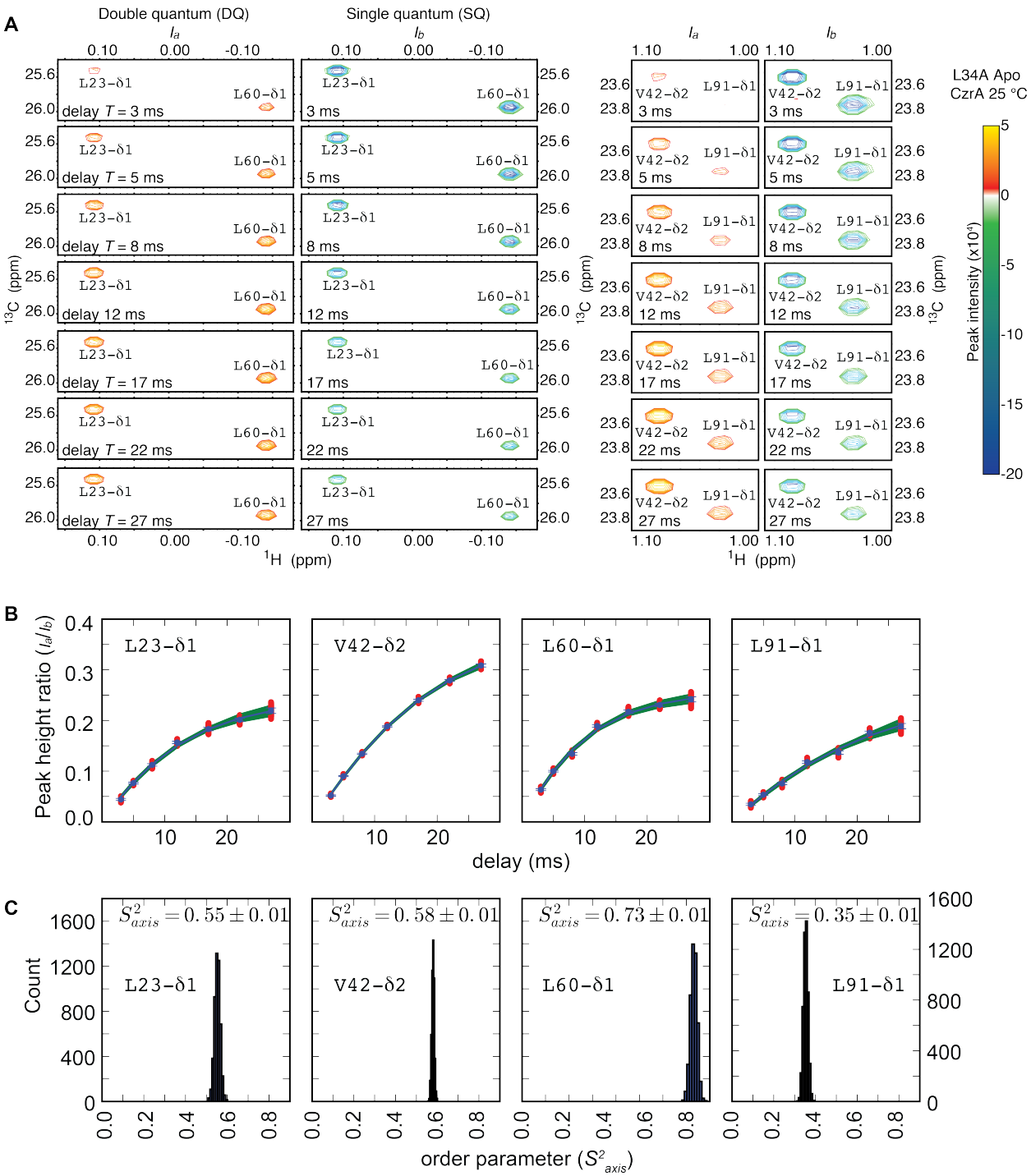

Figure S6. (A) Representative regions of 2D spectra acquired to obtain the order parameters of ILVAM residues for apo-L34A CzrA at 25°C. Plots show the time dependence of peak intensities in a correlated pair of single and double quantum experiments (see text for details) for four different methyl groups. (**B**) I_a/I_b ratio determined from panel **A** for the four methyl groups (blue circles; blue error bar from spectral noise and blue lines represent fitting to equation (6)) and the Monte Carlo fitting (red circles depict Monte Carlo simulated data based on the spectral noise and green lines represent single fits to Monte Carlo simulated data). (**C**) The distribution of Monte Carlo simulated S^2_{axis} values of the four methyl groups.

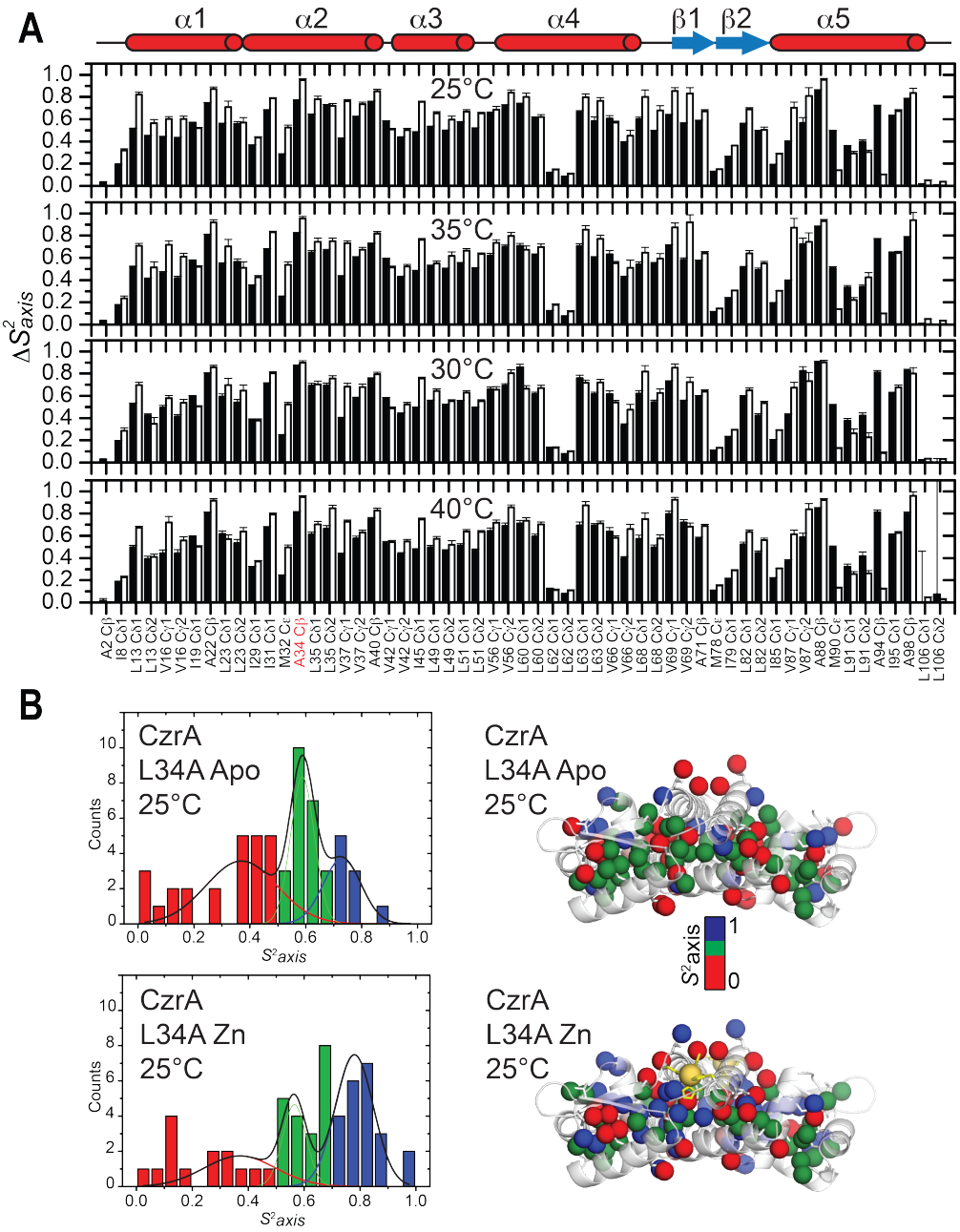

Figure S7. (**A**) Axial order parameters (S^2_{axis}) of individual methyl groups for L34A CzrA presented in a bar chart format at different temperatures for apo (black) and Zn^{2+} (white). (**B**) Histogram plot of S^2_{axis} from fitting the apo (top) and Zn-bound (bottom) states of L34A CzrA at 25°C calculated according to reference [7]. Absolute values of methyl group order parameters, S^2_{axis} on the methyl-bearing residues painted on the protein structure.

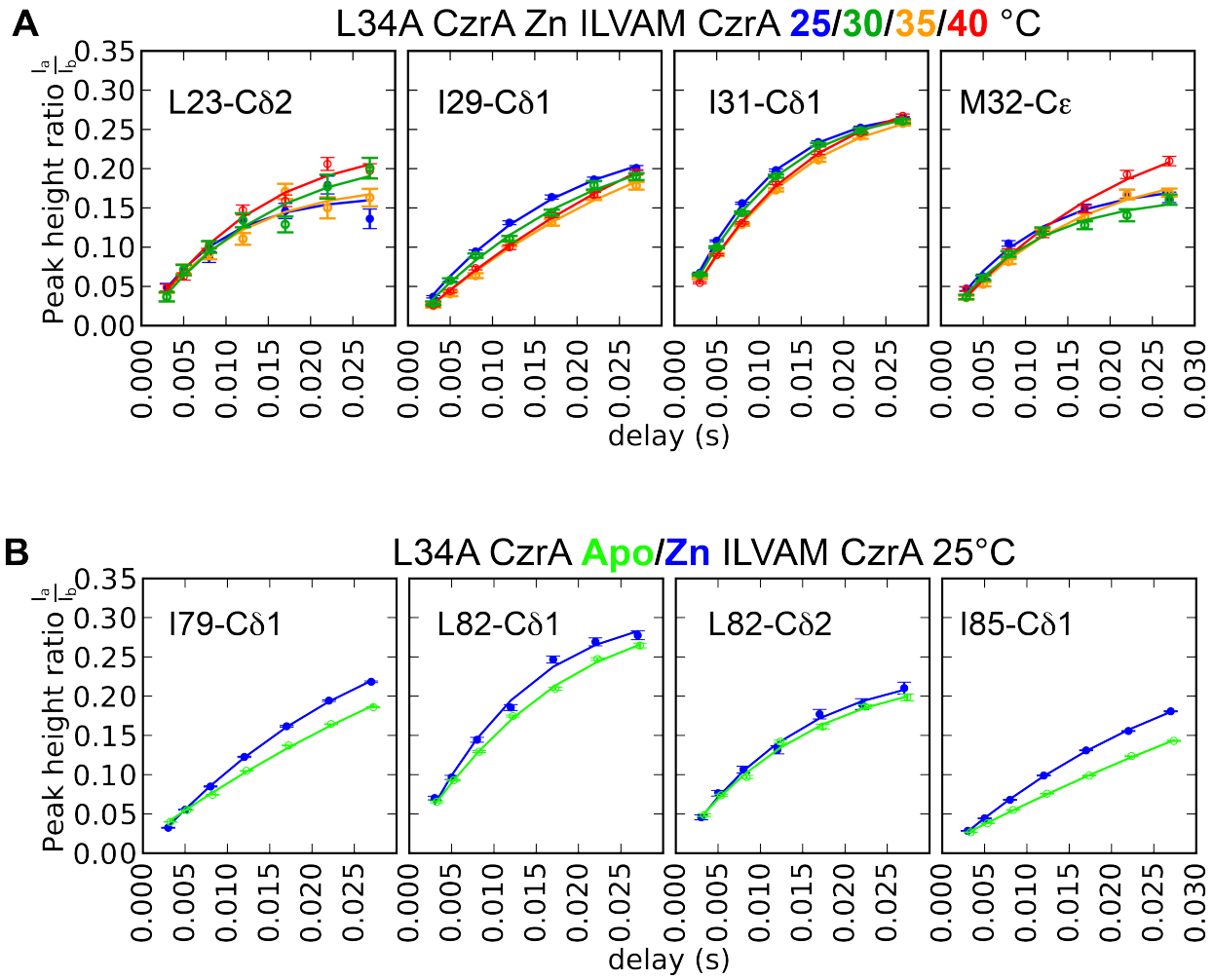

Figure S8. Axial order parameter (S^2_{axis}) analysis for representative methyl groups in L34A CzrA. Effect of temperature (**A**) and Zn binding (**B**) on I_a/I_b ratio used to obtain S^2_{axis} of selected ILVAM residues as described in Figure S6.

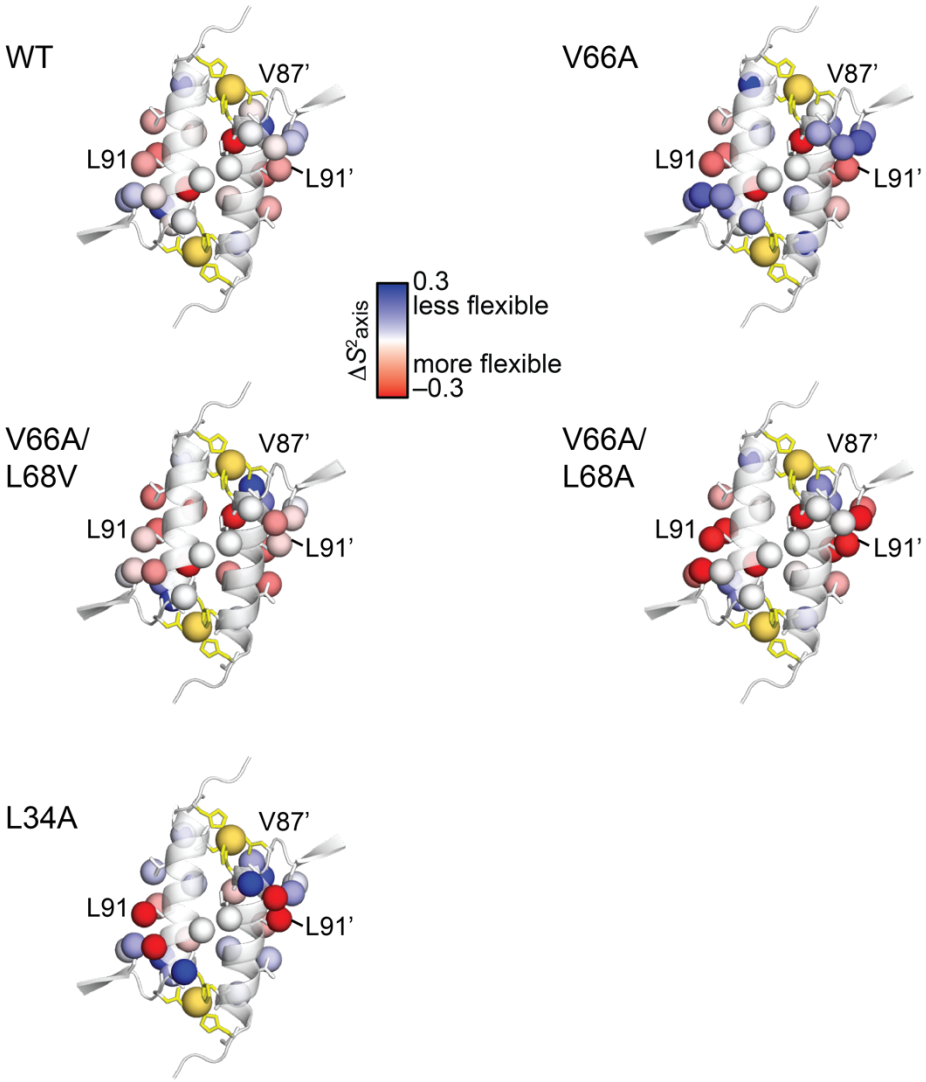

Figure S9. Local dynamics effects of Zn binding on CzrA variants. Change in order parameter (ΔS^2_{axis}) upon Zn binding painted onto spheres representing methyl groups on ribbon representations of the crystal structure of Zn-bound CzrA (PDB ID code 1r1v), with metal-binding residues shown as sticks and shaded *light yellow*, and Zn ions shown as yellow spheres.

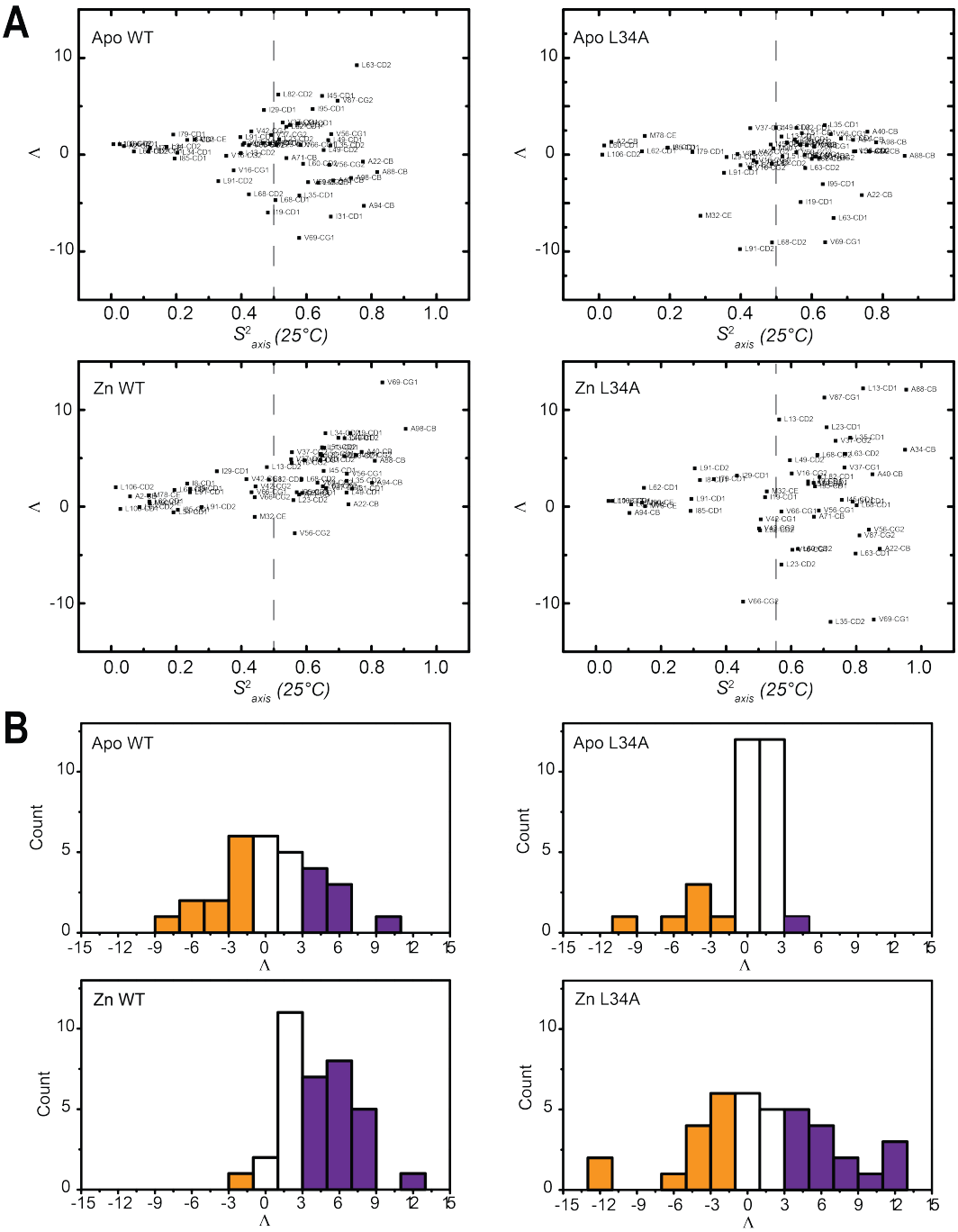

Figure S10. (**A**) Λ value against S^2_{axis} at 25°C; for Zn-loaded (*bottom*) and apo-states (*top*) for wild-type (*left*) and L34A (*right*) CzrAs. (**B**) Histograms of the Λ value obtained with equation (7) for residues with order parameters higher than 0.5 or Zn-loaded (*bottom*) and apo-states (*top*) for wild-type (*left*) and L34A (*right*) CzrAs.

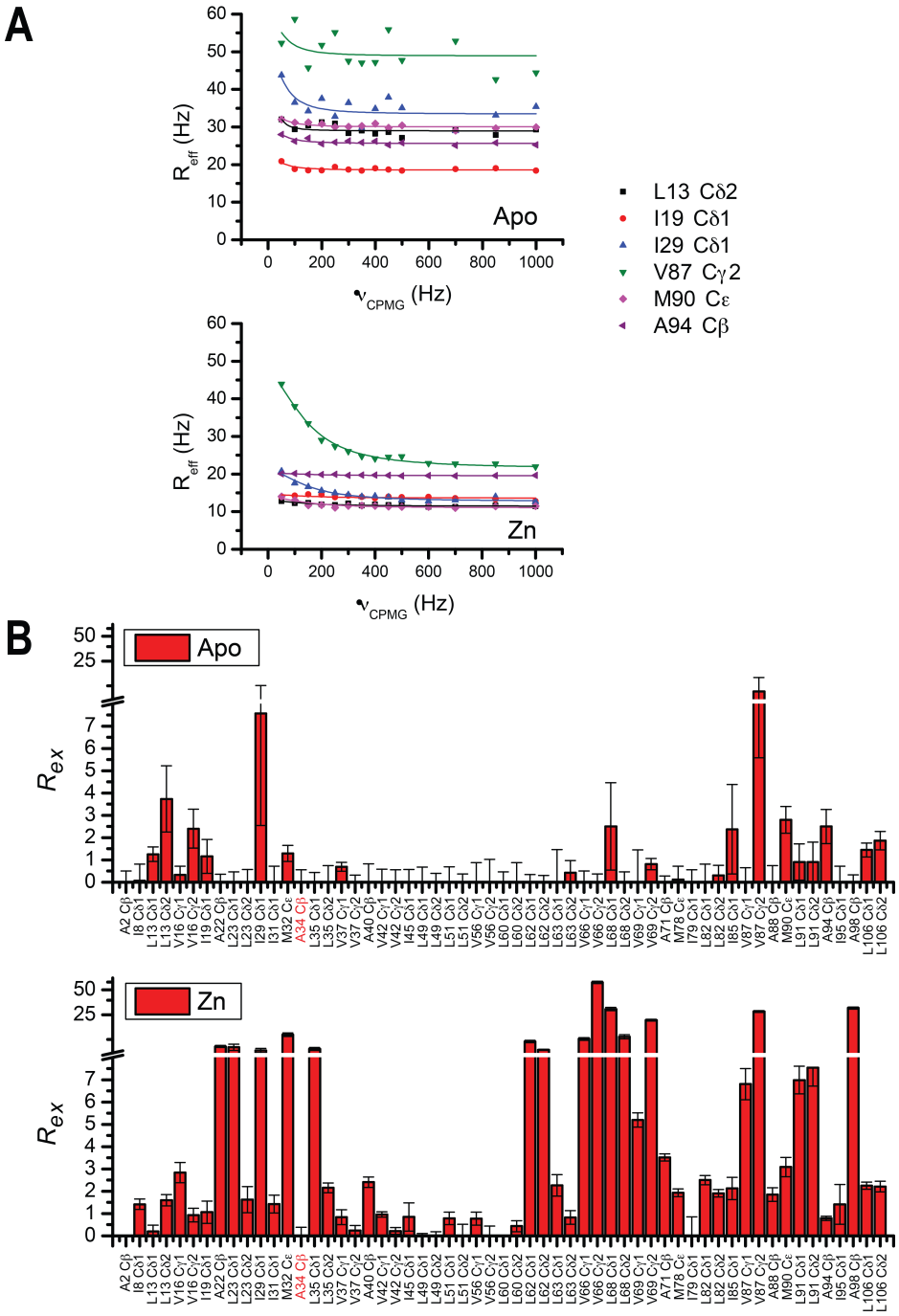

Figure S11. (**A**) Representative raw relaxation dispersion curves used to determine R_{ex} for the indicated methyl groups. (**B**) R_{ex} for both allosteric states are shown in each panel.

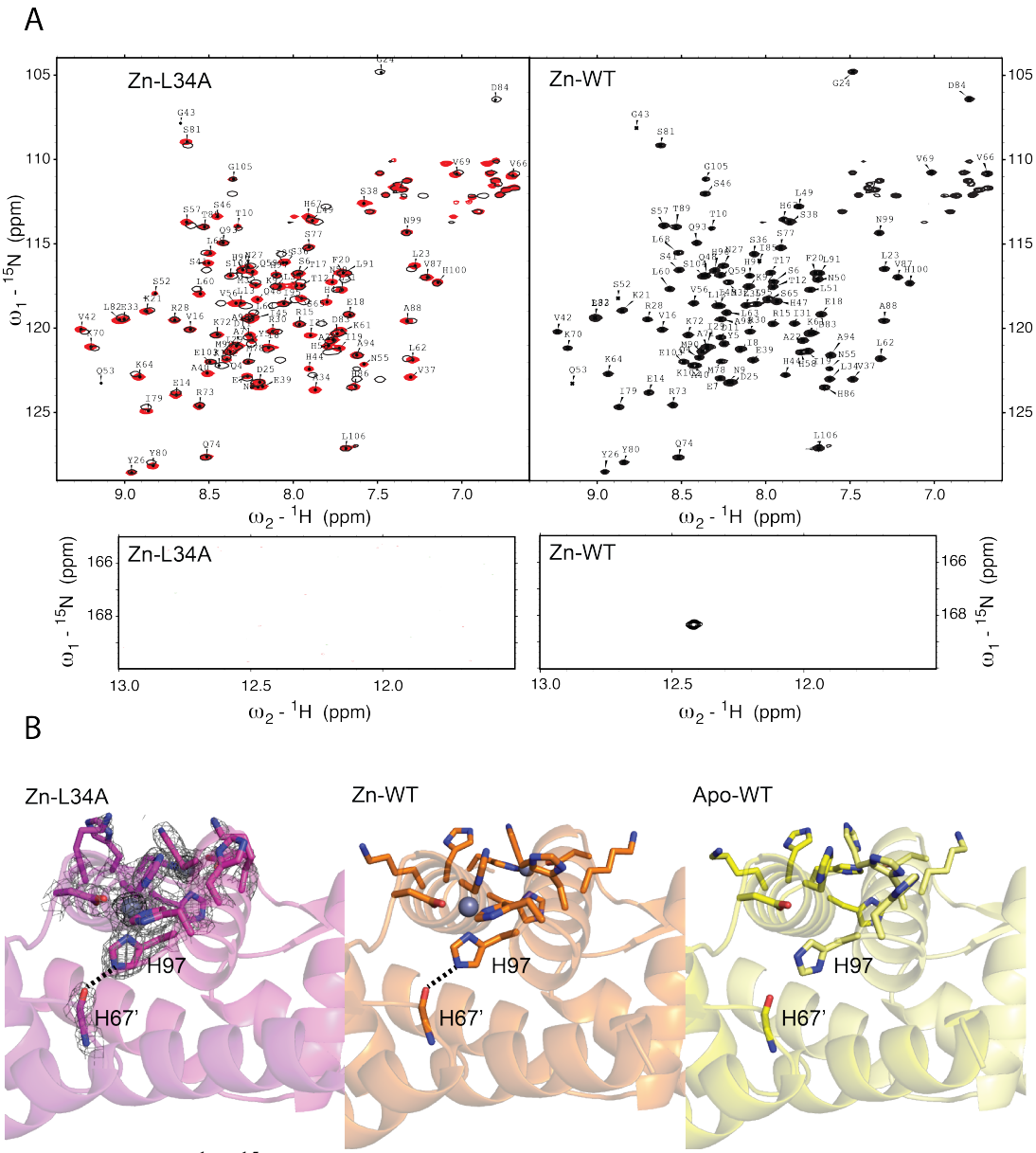

Figure S12. (**A**) ^{1}H-^{15}N HSQC spectrum of the backbone amide groups (*top*) and His 97 $N^{\varepsilon 2}$-$H^{\varepsilon 2}$ correlation (*bottom*) in L34A and wild-type CzrAs in the Zn-bound state. (**B**) H-bond between H67' backbone and H97 sidechain is shown as a dashed line in Zn-bound L34A CzrA and the wild-type CzrA crystal structures. The apo-CzrA wild-type structure is shown on the right for comparison. Anomalous density on Zn atoms (*black*) is shown on the L34A CzrA crystal structure (see Table S4 for statistics). Note that this hydrogen bond is present in the crystal structure (Fig. 2A and S10) which emphasizes the difficulties of predicting dynamic behavior from crystallographic structures. The modelling of the crystal structure slightly favors the rotameric state of the His presented in panel B; however, with the current resolution it is not possible to ensure the presence of this H-bond in the crystal structure and NMR provides the most compelling evidence of the presence of this H-bond in wild-type and other CzrA variants.

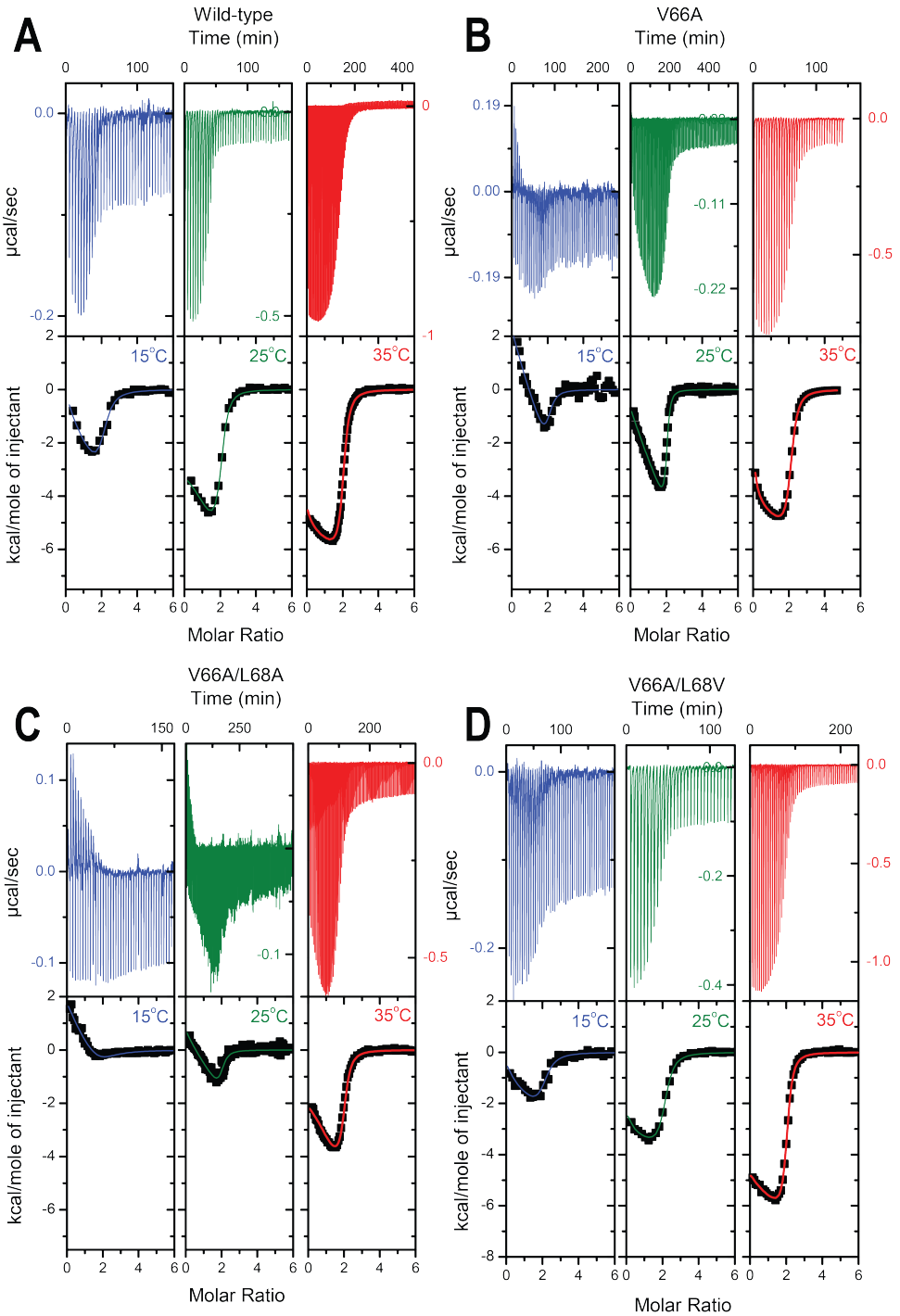

Figure S13. Titration of Zn^{2+} into apo-CzrA dimers (**A**, wild-type; **B**, V66A; **C**, V66A/L68A; **D**, V66A/L68V) in 50 mM HEPES, 400 mM NaCl pH 7.0, 5.0 mM NTA. The top panel shows the raw data plotted as power vs time and the bottom panel is the integrated, concentration-normalized ITC data. The continuous line indicates the best fit according to a two-site sequential binding model.

Appendix 1 – Metal dehydration entropy

A significant contribution to the solvent entropy of Zn(II) binding derives from the net disordering of metal-coordinated water molecules after the protein sequesters each Zn(II) ion from the solution. This effect is known as the chelation effect and originates with the hydration of metal ions in solution. The release of this hydration shell upon formation of the protein-derived coordination complex is thus represented by:

$$Zn(H_2O)_6{}^{+2} + X_4Lig \rightarrow ZnX_4Lig^{+2} + 6\ H_2O \qquad \text{(S1)}$$

where X_4Lig is a ligand that forms four coordination bonds with the metal and Zn^{2+} is hydrated by 6 water as demonstrated with several techniques[8].

In the case of CzrA, Zn binding also results in the exchange of one net Zn(II) for a proton at pH 7.0[3]; thus, the metal dehydration process can be represented by the reaction:

$$2\ Zn^{+2}\ (aq) + H_2X_8Lig \rightarrow Zn_2X_8Lig + 2\ H^+\ (aq) \qquad \text{(S2)}$$

for which the ΔG and $-T\Delta S$ (derived from eq. S3, eq. 1 and from the Gibbs-Helmholtz equation) can be written as follows and evaluated in the conditions of the ITC experiments (50 mM HEPES, 400 mM NaCl, pH=7.0, 25°C):

$$\Delta G_{SOLV}^{metal-dehydration} = 2\left[\Delta\bar{G}° + RT\ln\frac{[H^+]\gamma_{H+}}{[Zn^{2+}]\gamma_{Zn2+}}\right] \qquad \text{(S3)}$$

$$-T\Delta S_{SOLV}^{metal-dehydration} = 2\left[-T\Delta\bar{S}° + RT\ln\frac{[H^+]\gamma_{H+}}{[Zn^{2+}]\gamma_{Zn2+}} + RT^2\left.\frac{\partial\left(\ln\frac{\gamma_{H+}}{\gamma_{Zn2+}}\right)}{\partial T}\right|_p\right]$$

$$= -11.4\ \text{kcal mol}^{-1} \qquad \text{(S4)}$$

where $-T\Delta\bar{S}°$ can be calculated from the standard hydration of Zn^{2+} with respect to proton (-111 J mol^{-1} K^{-1})[9,10] giving a value of –7.9 kcal mol^{-1}; $[H^+] = 10^{-7}$M; free Zn, $[Zn^{2+}] = 0.9 \times 10^{-8}$M calculated from the total metal ion concentration (2.5 mM) and the competition values ($\Omega = 6.0 \times 10^5$ at 5.0 mM NTA, see ref. [11] for a detailed derivation of this value); the proton activity

coefficient, $\gamma_{H+} = 0.733$, previously reported for trace HCl in NaCl solution with I = 0.3809 M using the Harned cell[12]; and the Zn activity coefficient, $\gamma_{Zn2+} = 0.45 \pm 0.05$ based on the values reported for $ZnCl_2$ solutions with I = 0.4 M from Pitzer equation[13,14]. Based on the small differences shown for γ_{H+} with changes in temperature (0.743 at 5°C and 0.722 at 45°C)[12], we conclude that the third term in eq. S4 is a negligible contributor to the $-T\Delta S$ for the metal dehydration process. The value obtained is similar to the entropy for Zn(II) binding with the same geometry to a small molecule, such as triethylenetetramine (trien, $-T\Delta\bar{S}$ = –6.6 kcal mol^{-1} at I = 0.1 M, 25°C)[15].

Assuming that the activity coefficients' dependencies on temperature are negligible[12] compared to the $\Delta\overline{Cp}°$ (93 J mol^{-1} K^{-1})[16], the temperature at which this entropy becomes 0 can be estimated to be 94K ($T_S^{metal-dehydration}$), using an expression similar to eq. 9:

$$-T\Delta\bar{S}_{SOLV}^{metal-dehydration} = -T\left[\Delta\overline{Cp}_{SOLV}\ln\left(\frac{T}{T_S^{metal-dehydration}}\right)\right] \quad \text{(S5)}$$

This value is significantly lower than 0°C and lower than the previously determined values for polar solvation entropies (176 K[17] and 335 K[18]) which is expected from the obtained temperature dependence for other ions[19].

Appendix 2 – Solvent entropy calculation

Historically, the solvent entropy of protein binding and protein folding has been calculated from the hydration heat capacity contributions, generally classified into polar and apolar, and experimentally determined reference temperatures at which solvation entropies extrapolate to 0 (T_S), as follows:

$$-T\Delta S_{SOLV} = -T\left[\Delta Cp_{apolar}\ln\left(\frac{T}{T_S^{apolar}}\right) + \Delta Cp_{polar}\ln\left(\frac{T}{T_S^{polar}}\right)\right]$$

$$= -T \left[\Delta\widetilde{Cp}_{apolar} \Delta ASA_{apolar} \ln\left(\frac{T}{T_S^{apolar}}\right) + \Delta\widetilde{Cp}_{polar} \Delta ASA_{polar} \ln\left(\frac{T}{T_S^{polar}}\right) \right] \quad \text{(S6)}$$

where ΔCp represent the change in different hydration heat capacities in a particular reaction, $\Delta\widetilde{Cp}$ in changes in hydration heat capacities per unit area[2], T_S^{apolar} and T_S^{polar} have been determined in general from extrapolation of the solvation entropy dependence of different aminoacids[17], small molecules[20] and protein unfolding[18]. This approach of obtaining solvent entropy assumes additivity of the different hydration entropy terms and is generally used to estimate solvent entropies in protein binding and folding when changes in the ASA are the major contributors to the solvent entropy[2,7,18,21]. However, in the case of CzrA, where the structure of the unligated and metal bound forms show minimal structural differences, it is not possible to accurately determine ΔCp_{apolar} and ΔCp_{polar} because the changes in the ASA determined from the crystal structures are not representative of the overall thermodynamics (Table S4 and Fig. 1C). Moreover, eq. S6 is incomplete in this case because additional heat capacity contributions related to the metal and proton exchange has to be taken into account (Appendix 1). To avoid the complication of dissecting the solvent entropy term and to obtain an independent measurement of the solvent entropy for the CzrA variants relative to wild-type, we took a simpler formulation of the solvent entropy terms. eq. (S6) was rewritten in a more general way with no assumptions:

$$-T\Delta S_{SOLV} = -T \left[\Delta Cp_{SOLV} \ln\left(\frac{T}{T_S}\right) \right] \quad \text{(9, main text)}$$

where the solvent entropy contribution for each CzrA variant ($-T\Delta S_{SOLV}$) is determined from:

- the solvent heat capacity (ΔCp_{SOLV}) for each CzrA was assumed to be comparable to the total heat capacity obtained from calorimetry. This assumption is supported by the crystal structures presented here and in previous work[20], molecular dynamics simulations[22] and backbone order parameter measurements[23] that suggest that the contributions of the main chain to the difference in calorimetric heat capacities upon metal binding are minor and can be considered negligible. This can be confirmed also by the conformational heat capacities of metal binding obtained from the temperature dependence of S^2_{axis} using methyls groups as reporters, which are below 8% of the total ΔCp (Table S5), as expected from similar results on other systems[2].

- the reference temperature at which solvation entropy is 0 (T_S = 396K) was determined from wild-type CzrA thermodynamics and dynamics measurements. The solvent entropy was obtained from the difference between the total and the conformational entropy (Fig. 1C). The ΔCp_{SOLV} from the difference between the total heat capacity previously obtained from calorimetry (ΔC_p=340 cal mol^{-1} K^{-1})[3] and the conformational heat capacity (Table S5, from temperature dependence of S^2_{axis}). The obtained T_S is not expected to change by mutation between hydrophobic amino acids that conserve the protein structure[24], even when these affect the total entropy and the heat capacity of metal binding. It should also be noted that this value is similar to the reported values for apolar surfaces (377K to 391K)[17,18,20] and much higher than the T_S expected for the metal term (94K, Appendix 1), thus suggesting a strong, non-additive effect of solvent interaction, as expected in electrostatic and polar interactions[18,25].

REEFERENCES

(1) Capdevila, D. A.; Braymer, J. J.; Edmonds, K. A.; Wu, H.; Giedroc, D. P. *Proc. Natl. Acad. Sci. U. S. A.* **2017**, *114*, 4424.
(2) Caro, J. A.; Harpole, K. W.; Kasinath, V.; Lim, J.; Granja, J.; Valentine, K. G.; Sharp, K. A.; Wand, A. J. *Proc. Natl. Acad. Sci.* **2017**, *114*, 6563.
(3) Grossoehme, N. E.; Giedroc, D. P. *J. Am. Chem. Soc.* **2009**, *131*, 17860.
(4) Willard, L.; Ranjan, A.; Zhang, H.; Monzavi, H.; Boyko, R. F.; Sykes, B. D.; Wishart, D. S. *Nucleic Acids Res.* **2003**, *31*, 3316.
(5) Pennella, M. A.; Shokes, J. E.; Cosper, N. J.; Scott, R. A.; Giedroc, D. P. *Proc. Natl. Acad. Sci. U. S. A.* **2003**, *100*, 3713.
(6) Campanello, G. C.; Ma, Z.; Grossoehme, N. E.; Guerra, A. J.; Ward, B. P.; Dimarchi, R. D.; Ye, Y.; Dann, C. E.; Giedroc, D. P. *J. Mol. Biol.* **2013**, *425*, 1143.
(7) Marlow, M. S.; Dogan, J.; Frederick, K. K.; Valentine, K. G.; Wand, A. J. *Nat. Chem. Biol.* **2010**, *6*, 352.
(8) Ohtaki, H.; Radnai, T. *Chem. Rev.* **1993**, *93*, 1157.
(9) Burgess, J. In *Ions in Solution*; Elsevier, 1999; pp 45–61.
(10) Marcus, Y.; Loewenschuss, A. *Annu. Reports Sect. "C" (Physical Chem.* **1984**, *81*, 81.
(11) Grossoehme, N. E.; Giedroc, D. P. In *Springer*; Bujalowski, W., Ed.; 2012; Vol. 875, p 397.
(12) Macaskill, J. B.; Robinson, R. A.; Bates, R. G. *J. Solution Chem.* **1977**, *6*, 385.
(13) Miladinović, J.; Ninković, R.; Todorović, M.; Jovanović, V. *J. Chem. Thermodyn.* **2003**, *35*, 1073.
(14) Rard, J. A.; Miller, D. G. *J. Chem. Thermodyn.* **1989**, *21*, 463.
(15) Grossoehme, N. E.; Akilesh, S.; Guerinot, M. Lou; Wilcox, D. E. *Inorg. Chem.* **2006**, *45*, 8500.
(16) Marcus, Y. *J. Chem. Soc., Faraday Trans.* **1993**, *89*, 713.
(17) Privalov, P. L.; Makhatadze, G. I. *J. Mol. Biol.* **1993**, *232*, 660.
(18) D'Aquino, J. A.; Gómez, J.; Hilser, V. J.; Lee, K. H.; Amzel, L. M.; Freire, E. *Proteins* **1996**, *25*, 143.
(19) Gates, J. A.; Tillett, D. M.; White, D. E.; Wood, R. H. *J. Chem. Thermodyn.* **1987**, *19*, 131.
(20) Baldwin, R. L. *Proc. Natl. Acad. Sci.* **1986**, *83*, 8069.
(21) Hilser, V. J.; García-Moreno E, B.; Oas, T. G.; Kapp, G.; Whitten, S. T. *Chem. Rev.* **2006**, *106*, 1545.
(22) Chakravorty, D. K.; Wang, B.; Lee, C. W.; Giedroc, D. P.; Merz, K. M. *J. Am. Chem. Soc.* **2012**, *134*, 3367.
(23) Arunkumar, A. I.; Campanello, G. C.; Giedroc, D. P. *Proc. Natl. Acad. Sci. U. S. A.* **2009**, *106*, 18177.
(24) Makhatadze, G. I.; Privalov, P. L. *J. Mol. Biol.* **1993**, *232*, 639.
(25) Spolar, R. S.; Record, M. T. *Science* **1994**, *263*, 777.